



Article

Experimental Measurements of Explosion Effects Propagating in the Real Geological Environment—Correlation with Small-Scale Model

Daniel Papán ^{1,2,*} , Emma Brozová ¹ and Zuzana Papánová ¹ 

¹ Department of Structural Mechanics and Applied Mathematics, Faculty of Civil Engineering, University of Žilina, Univerzitná 8215/1, 010 26 Žilina, Slovakia; emma.brozova@uniza.sk (E.B.); zuzana.papanova@uniza.sk (Z.P.)

² Department of Materials and Structures, Institute of Construction and Architecture, Slovak Academy of Sciences, Dúbravská cesta 9, 845 03 Bratislava, Slovakia

* Correspondence: daniel.papan@uniza.sk; Tel.: +421-948-037947

Abstract: This research focuses on comparing small-scale and full-scale measurements of wave propagation from explosions by using scaling relationships to find significant correlations between the two. The study investigates how seismic waves generated by explosions behave in the geological environment. The research covers various aspects such as the development of the model, the explosive materials used, measurement methods, evaluation techniques, and relevant software. A scientific approach based on the principle of backward Fourier transform was used to process and evaluate the data, which helps to filter the frequencies. One of the important calculations discussed is the determination of the attenuation coefficient, which helps to describe how waves attenuate as they pass through a material. The research also deals with dynamic scaling, using the dynamic exponent as a scaling factor to provide a better understanding of the behavior of waves at different scales. By comparing real in situ data with results from small-scale models, the study provides a robust framework for predicting the effects of explosions in complex geological environments. The research results show a high correlation coherence of the statistical data files of up to 4.1%. For dynamic tasks and model scaling, an important result can be pointed out, namely the approximately fourfold decrease in the exponents of the dependence on the distance from the excitation source and the amplitudes between P-waves (0.4316) and R-waves (0.1219). Conclusions are targeted at the possibility of correlating three types of results: small-scale simulations, numerical simulations, and a real full-scale experiment.

Keywords: technical seismicity; explosions; dynamic scaling; attenuation; wave propagation



Citation: Papán, D.; Brozová, E.; Papánová, Z. Experimental Measurements of Explosion Effects Propagating in the Real Geological Environment—Correlation with Small-Scale Model. *Buildings* **2024**, *14*, 3603. <https://doi.org/10.3390/buildings14113603>

Academic Editor: Francisco López-Almansa

Received: 27 July 2023

Revised: 3 October 2024

Accepted: 18 October 2024

Published: 13 November 2024



Copyright: © 2024 by the authors. Licensee MDPI, Basel, Switzerland. This article is an open access article distributed under the terms and conditions of the Creative Commons Attribution (CC BY) license (<https://creativecommons.org/licenses/by/4.0/>).

1. Introduction

Technical seismicity is the field that studies and characterizes seismic waves generated by human activities such as mining, building, transportation, and industrial activities. Unlike seismicity induced by natural phenomena (e.g., geological processes), technical seismicity is due to artificial causes and is generally lower in intensity but much higher in frequency of occurrence.

While similar topics have been investigated in the past, no explicit correlation has ever been found between small-scale models and the real dynamic response of the geological environment to blast loading. Several high-quality publications are available [1–3].

This article deals with the topic of explosive seismicity, which has gained significant attention in recent years due to a variety of factors, including the ongoing conflict in Ukraine and the increasing number of terrorist attacks around the world [4,5]. Understanding the behavior of explosions and predicting their effects are of fundamental importance for the design and construction of structures that can withstand such extraordinary dynamic loads and enhance the safety of users and the entire infrastructure.

Dynamic loads differ from static loads in that they are time-varying, and the effects of inertial forces must also be taken into consideration. From the point of view of building structures, load frequencies between 0.1 and 500 Hz are crucial. The greatest damage occurs mainly in the frequency range from 1 to 150 Hz. The impact caused by an explosion has a frequency range from 1 to 40 Hz, and for this reason, it is also necessary to pay attention to this issue [6].

A chemical explosion is a reaction or change of state over a very short interval (in the μs range). The decomposition of a chemical substance results in the release of a large amount of energy, which is converted into work [7]. The energy released during an explosion propagates away from the source site in four main ways. Longitudinal P-waves (primary) reach the accelerometers first, followed by transverse S-waves (secondary), and last are surface waves (Love and Rayleigh waves), which have the most destructive effect due to the fact that up to 67% of the energy is transmitted by the Rayleigh wave [8].

2. Materials and Methods

2.1. Description of Measuring Equipment and Explosives Used

To conduct the actual experimental measurements, adequate equipment was needed. Appropriate selection of data-recording equipment is crucial to obtain accurate and reliable results. As shown in Figure 1, two essential types of equipment were used.



Figure 1. Equipment used for the measurements—accelerometer (**left**) and module (**right**). (a) Accelerometer B&K type 8340; (b) Module PULSE LAN-XI B&K type 3050-B-060.

Accelerometers—Brüel & Kjær piezoelectric accelerometer type 8340 is used for seismic measurements. This type of accelerometer is specially designed with high sensitivity for measurements at very low frequencies. The frequency range is from 0.1 to 1500 Hz [9].

Module—PULSE LAN-XI Brüel & Kjær type 3050-B-060 is a 6-channel module that is designed to cover the largest possible range of applications for sound and vibration measurements. It has a frequency range from 0 to 51.2 kHz [10].

Explosives are substances that undergo a rapid chemical reaction that releases large amounts of energy in the form of heat, light, and gas. They can be used for a wide range of applications, from mining and civil engineering to military and terrorist activities. Firecrackers are classified into four categories (F1, F2, F3, and F4) depending on their use, purpose, and hazard level [11]. The first three categories are commonly available to the public, but professional pyrotechnics of category F4 are only for use by qualified experts. For the purpose of experimental measurements, Dum Bum cat. F2, Megatresk cat. F3, Viper 1 cat. F3 firecrackers (Figure 2), and V10b-el military explosives were used (Figure 3).

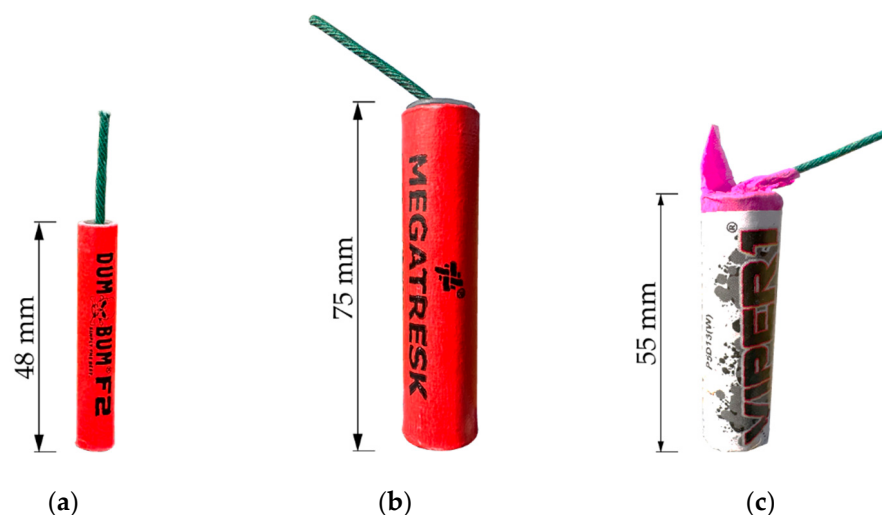


Figure 2. Types of firecrackers used in experimental measurements. (a) Dum Bum cat. F2; (b) Megatresk cat. F3; (c) Viper 1 cat. F3.

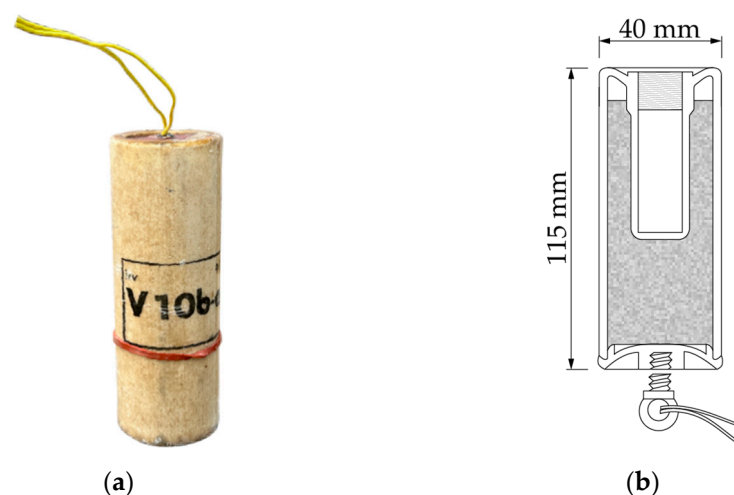


Figure 3. V10b-el military explosive (a) and its vertical section (b). (a) Explosive V10b-el; (b) Vertical section of the explosive.

Megatresk contains only a flash component of 1.0 g on the principle of potassium perchlorate KClO_4 and Al (aluminium powder) in a 7:3 ratio. This pyrotechnic composition is homogenized (mixed) using a special device.

Military explosive V10b-el—the external part of the explosive—is made of a waxed paper body, which the charge consists of barium nitrate $\text{Ba}(\text{NO}_3)_2$, potassium perchlorate KClO_4 , and aluminium powder Al with a total weight of these pyrotechnic components of 40.0 g.

2.2. Calibration of Accelerometers

Calibration measurements are an important aspect of ensuring the accuracy and reliability of results. Calibration involves comparing accelerometer data with a known standard to verify that the accelerometers are functioning correctly and providing accurate measurements. They help to identify potential problems and sources of error, which can then be addressed to improve the accuracy and reliability of the entire system.

The calibration was performed to verify the accuracy of the measurements of the B&K type 8340 accelerometers. In this process, the B&K type 4508 reference accelerometer was attached to the calibration pad while the B&K type 8340 accelerometers were changed. A total of four measurements were made, each time outputting the same sinusoidal sweep

signal ranging from 0 Hz to 100 Hz. Sinusoidal signals are often used in calibration measurements because they are relatively simple and easy to generate and can be characterized by frequency, phase, and amplitude. The measurements were carried out using the PULSE system, where all the data collected was exported as a CSV file type that could then be worked with.

Figure 4 represents a graphical representation of the relationship between the data obtained from the B&K type 8340 accelerometer and the reference accelerometer B&K type 4508, which served as a known standard. In this case, the frequency range is from 0 Hz to 20 Hz.

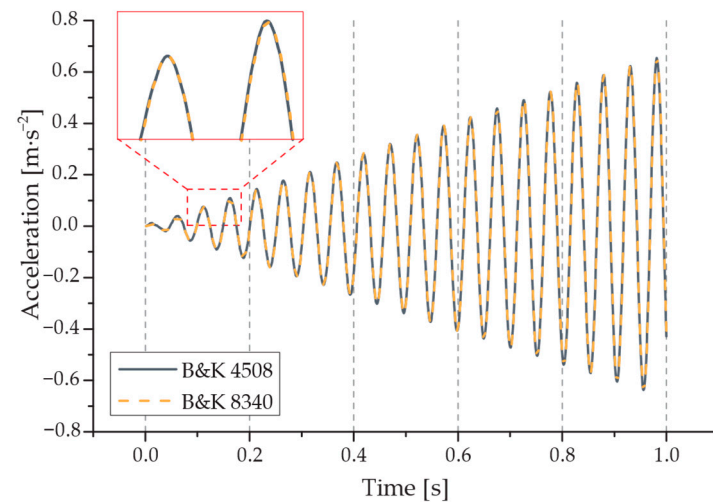


Figure 4. Example from calibration measurement No. 1—calibration curve for the frequency range from 0 Hz to 20 Hz.

Figure 5 shows the calibration measurement equipment, which consisted of a reference accelerometer attached to a vibration generator and a signal generator and amplifier used to generate a signal.

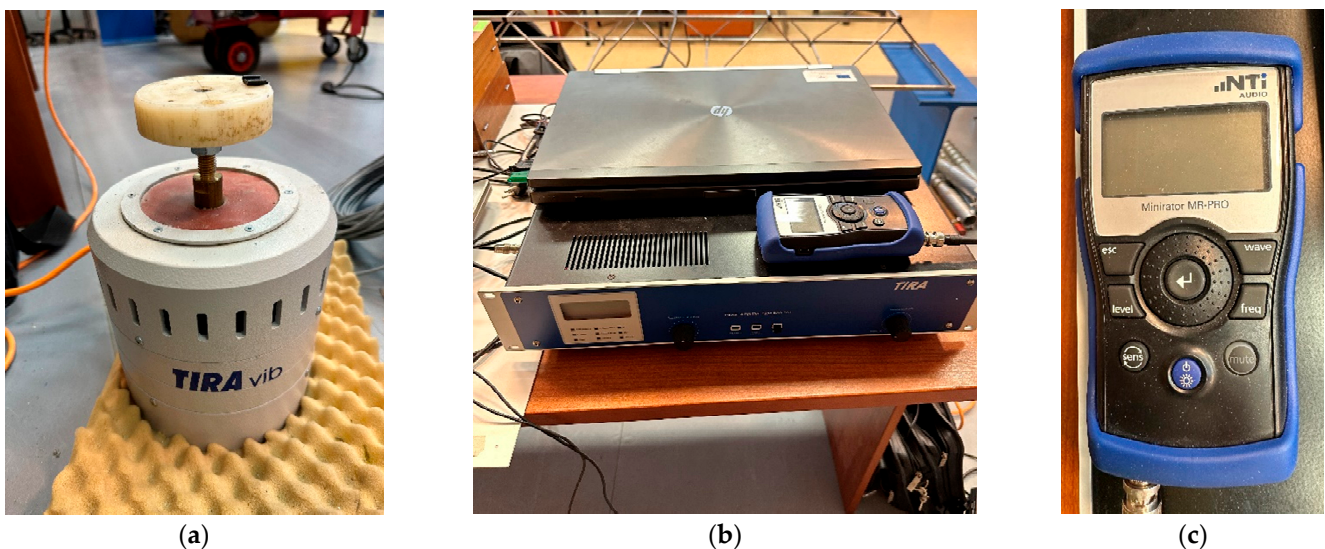


Figure 5. Equipment required to carry out calibration measurements. (a) TIRAvib vibration generator; (b) TIRA BAA 120 amplifier; (c) Miniator MR-PRO sound signal generator.

The analysis was carried out using the Pearson correlation coefficient, which is a frequently used method to determine the linear relationship between two variables. It is denoted by r and the coefficient represents a number between +1 and -1 that expresses

the strength and direction of the linear relationship. A positive result indicates a positive linear relationship (positive correlation), which means that as the value of one variable increases, the value of the other variable also increases. A negative number indicates a negative linear relationship (negative correlation), which means that when the value of one variable increases, the value of the other decreases. A value of 0 means that there is no linear relationship between the two variables [12].

The Python programming language was used to evaluate the relationship between one accelerometer and the other from all four measurements, which allowed a thorough and quick evaluation of the results. Its extensive features guaranteed the accuracy of the calculations and the clarity of the outputs, making it an ideal tool for this type of analysis. The two accelerometers were compared with each other and also with a theoretical signal, which was generated for all frequency ranges in SigView software (version 3.0.2.0) as a sweep signal that had to be derivatized twice (Figure 6).

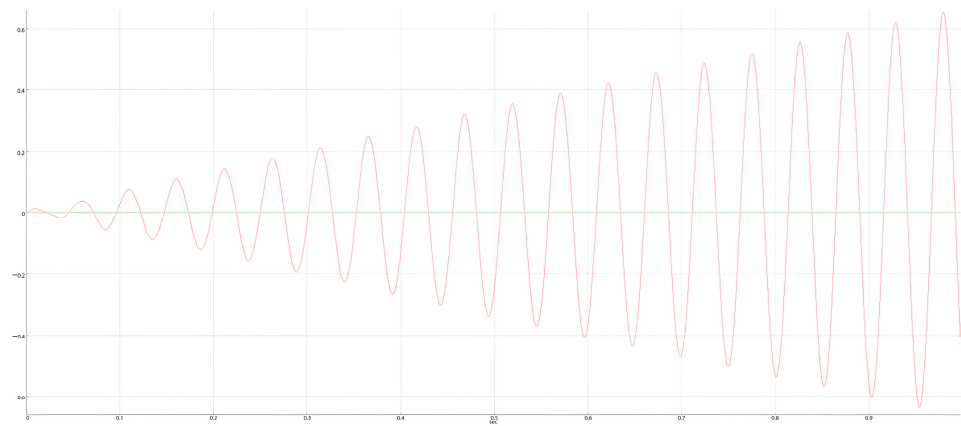


Figure 6. Two times derivative theoretical sweep signal generated in SigView software for amplitude range 0 Hz–20 Hz at sampling frequency $f_s = 1024$ Hz.

Figure 7 graphically represents the Pearson correlation coefficient values for the four calibration measurements. For the purpose of clarity, the B&K type 4508-B-002 accelerometer is labeled as A, the B&K type 8340 accelerometer is labeled as B, and the theoretical signal is labeled as C.

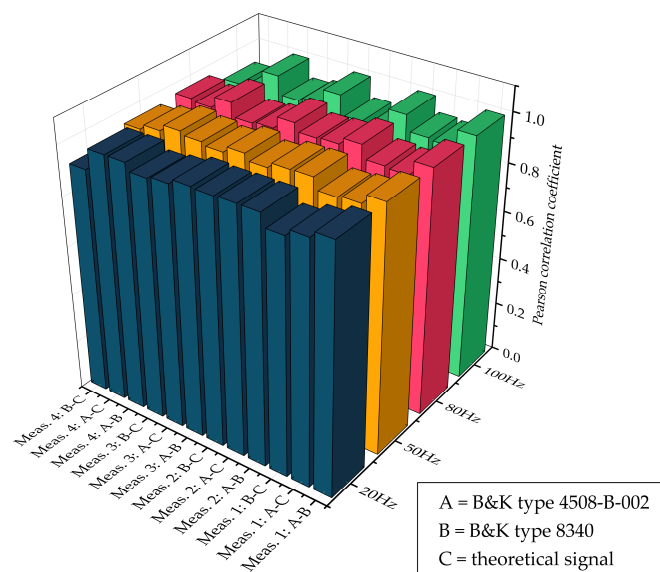


Figure 7. Graphical representation of Pearson correlation coefficient values for the calibration measurements.

In all cases, the obtained Pearson correlation coefficient varied from 0.91 to 0.99, which means that there is a very strong correlation between the accelerometers, and they are suitable for use in further measurements and will guarantee the accuracy of the collected data.

2.3. Measurement Methodology

The experimental measurements were carried out at a military shooting range in the village of Kamenná Poruba, located in Slovakia in the Žilina district in the Rajec basin (Figure 8). The average altitude is 484 m above sea level. The location of Kamenná Poruba was chosen as a result of cooperation with the army—the 5th Special Operations Regiment in Žilina—which resulted in the provision of adequate premises, pyrotechnics, and professional personnel. This cooperation allowed us to provide optimal conditions for the realization of the measurements and to guarantee their safety.



Figure 8. Geographical representation of Kamenná Poruba on the map of Slovakia.

The first step was to design a measurement setup consisting of four accelerometers placed 2.5 m, 7.5 m, 17.5 m, and 37.5 m away from the blast source, as shown in Figure 9. For the last two measurements (measurement No. 9 and measurement No. 10), the position of the source was shifted by 1 m and 2 m. As a result, the distance between the explosion source and the first accelerometer A2 changed to 3.5 m for measurement No. 9 and 4.5 m for measurement No. 10. To ensure the stability of the measurement points, 530 mm long wooden stakes were used to ensure the precise position of the accelerometers during all measurements. In addition, all components of the calibrated assembly were used to provide accurate and reliable measurement results.

To prevent the propagation of acoustic waves, the accelerometers were covered with insulation wool and a plastic crate, as can be seen in Figures 10 and 11. The cable of the accelerometer closest to the source of the explosion was additionally covered with sand for a distance of about 1.5 m. The accelerometers were connected to the module and a PC where the measurements were triggered and recorded in the PULSE Time Data Recorder system. This system enabled real-time recording and processing of the signals. A test measurement phase was carried out as part of the experiment to verify the correct functioning of the measurement setup. During this stage, a sampling frequency of 8192 Hz was established. The dynamic loads in the test phase were the explosions on the ground surface generated by lower explosive category firecrackers.



Figure 9. Orthophoto map showing the entire shooting range (left) and a scheme of the measurement setup showing the arrangement of accelerometers in the propagating wave path from the source of the explosion (right).

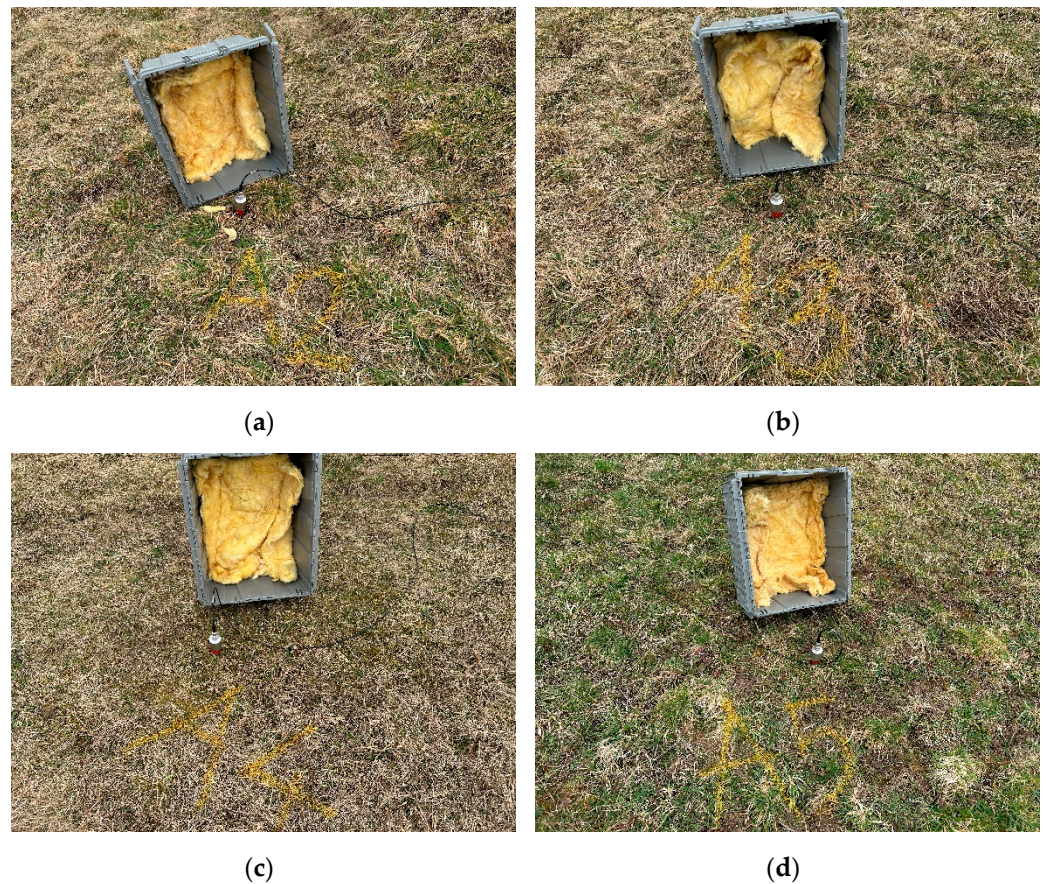


Figure 10. Accelerometer locations A2 to A5. (a) Accelerometer A2; (b) Accelerometer A3; (c) Accelerometer A4; (d) Accelerometer A5.



Figure 11. Placement of accelerometers in the direction away from the source of the explosion and in the path of the propagating waves.

After successful testing, 10 measurements were performed using three types of fire-crackers (Dum Bum, Megatresk, and Viper 1) and V10b-el military explosives (Figure 12). Each measurement was run manually in the PULSE Time Data Recorder and took a few seconds. The overall procedure of the experiment was very thorough and ensured high-quality measurements. All accelerometers were pre-calibrated to guarantee accurate and reliable results.



Figure 12. Image showing the explosion of a pair of V10b-el military explosives—measurement No. 10.

3. Results

To evaluate the measurement data, it was first essential to remove unnecessary data before and after the actual explosion event. This process was repeated for each measurement and accelerometer separately. The CSV file was imported into the software and then analyzed. The experimental measurements resulted in graphical outputs.

The following graphs (Figures 13–23) show the vibration velocity time histories that were obtained with accelerometers placed at certain distances from the source of the explosion. In each graph, the time axis is the same, but each accelerometer has its own acceleration axis, including its own scale. The time axis shows the interval over which the wave processes of the geological environment at the ground surface were recorded as the vertical component of the acceleration of the vibration. Rayleigh waves consist

of longitudinal and transverse motions whose amplitude decreases exponentially with increasing distance from the surface. It should also be noted that when a Rayleigh wave passes through a geological environment, the particles move along an elliptical path that is counterclockwise. The graphs show the time delay with which the seismic waves arrived at each accelerometer. The waves arrived first at the closest one and then, with a gradual delay, at the other accelerometers, depending on their distance from the source.

In the last measurement, No. 10 (Figures 22 and 23), two military explosives were detonated simultaneously. Even though an electrical method was used for blasting, it was not possible to ensure that both charges exploded at exactly the same time. It is for this reason that two maximum acceleration values appear in the graphs for each accelerometer with a time difference of a few hundredths of a second.

Additionally, the measurements were evaluated in terms of dispersive attenuation. Dispersive attenuation occurs in an environment that is not homogeneous, i.e., has different properties. As a consequence, waves that pass through such an environment propagate with different velocities and are dispersed, leading to a gradual attenuation of the wave. The highest values can be observed closer to the source of the explosion and the acceleration values decrease as the distance from the source increases.

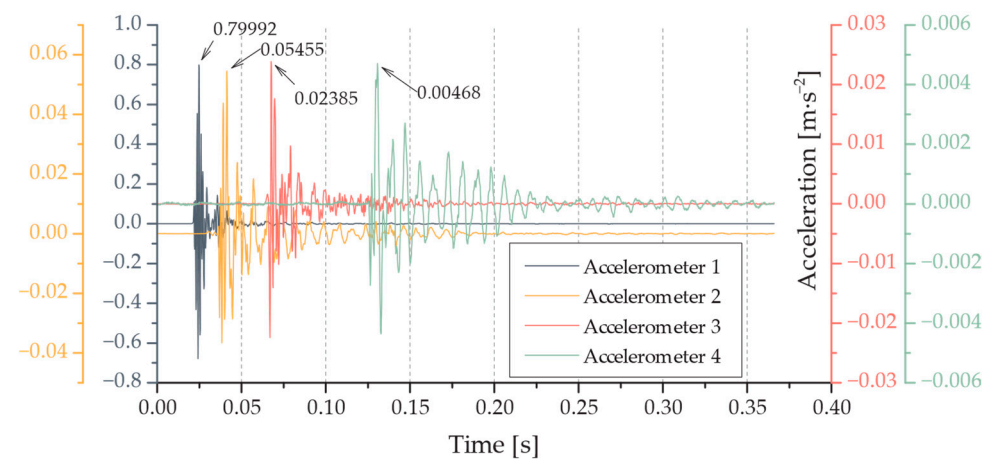


Figure 13. Measurement No. 1—firecracker Dum Bum cat. F2—vibration velocity time history of accelerometers 1 to 4 with indication of maximum acceleration values.

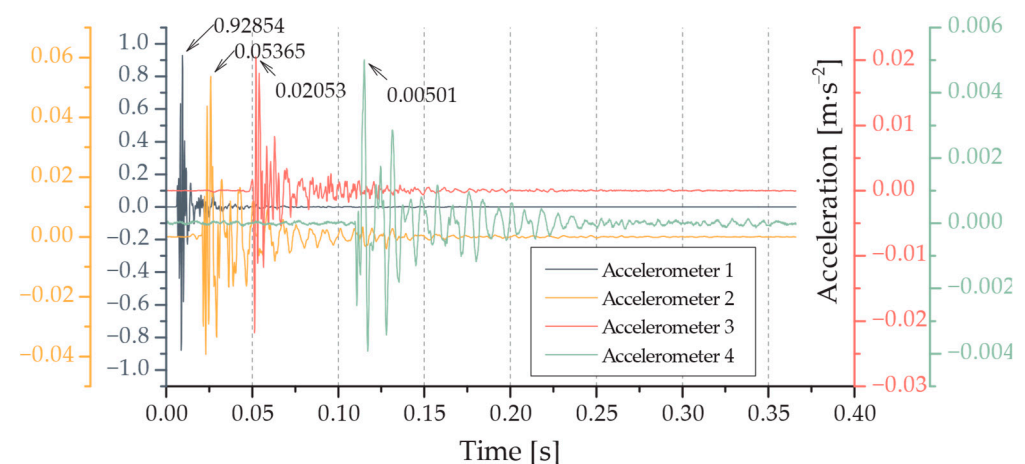


Figure 14. Measurement No. 2—firecracker Dum Bum cat. F2—vibration velocity time history of accelerometers 1 to 4 with indication of maximum acceleration values.

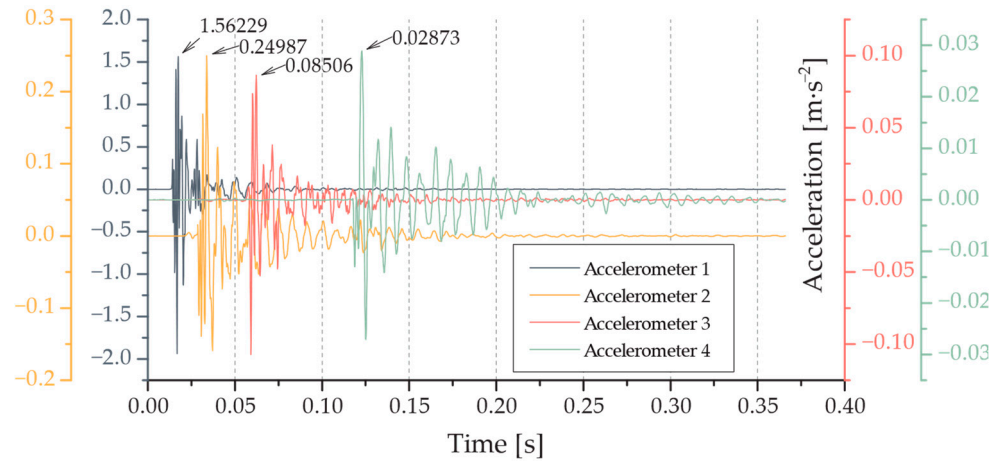


Figure 15. Measurement No. 3—firecracker Megatresk cat. F3—vibration velocity time history of accelerometers 1 to 4 with indication of maximum acceleration values.

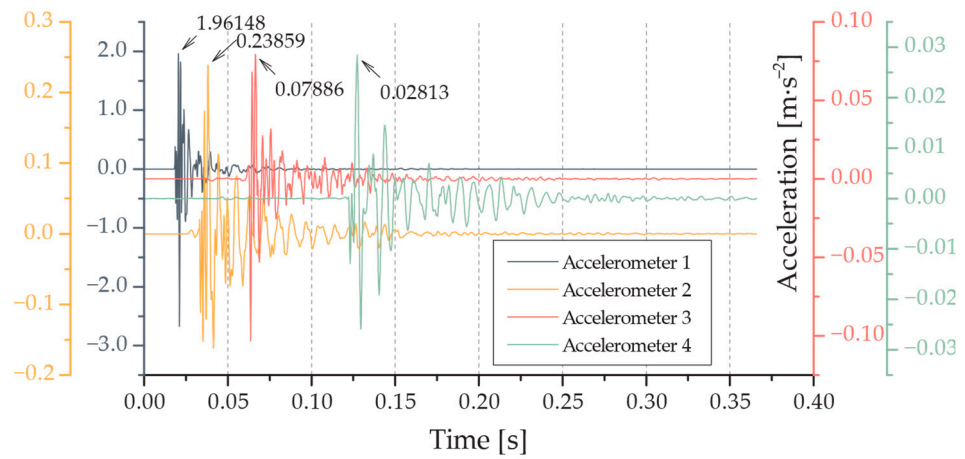


Figure 16. Measurement No. 4—firecracker Megatresk cat. F3—vibration velocity time history of accelerometers 1 to 4 with indication of maximum acceleration values.

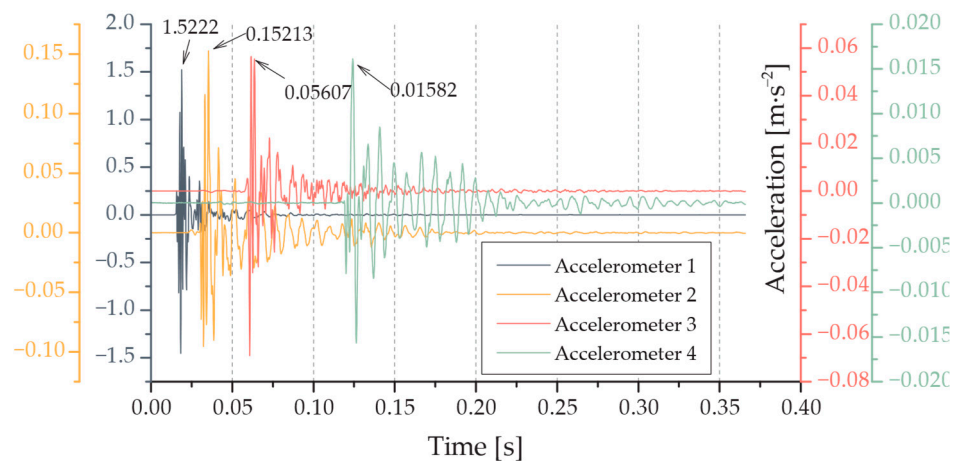


Figure 17. Measurement No. 5—firecracker Viper 1 cat. F3—vibration velocity time history of accelerometers 1 to 4 with indication of maximum acceleration values.

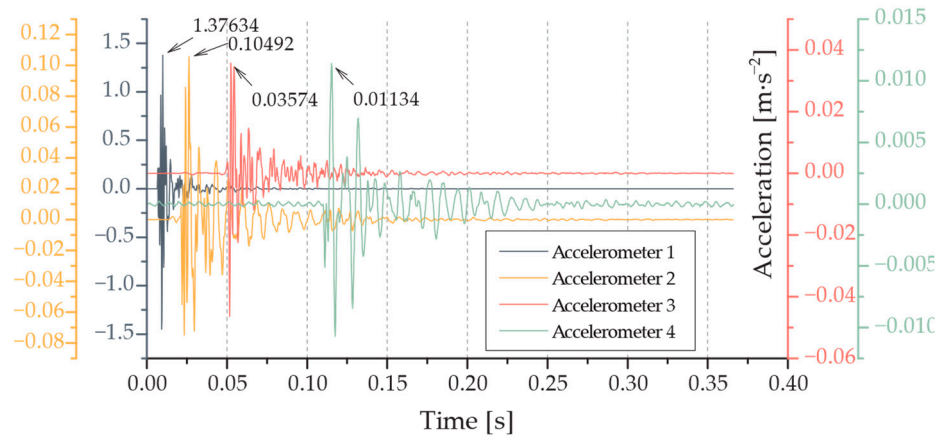


Figure 18. Measurement No. 6—firecracker Viper 1 cat. F3—vibration velocity time history of accelerometers 1 to 4 with indication of maximum acceleration values.

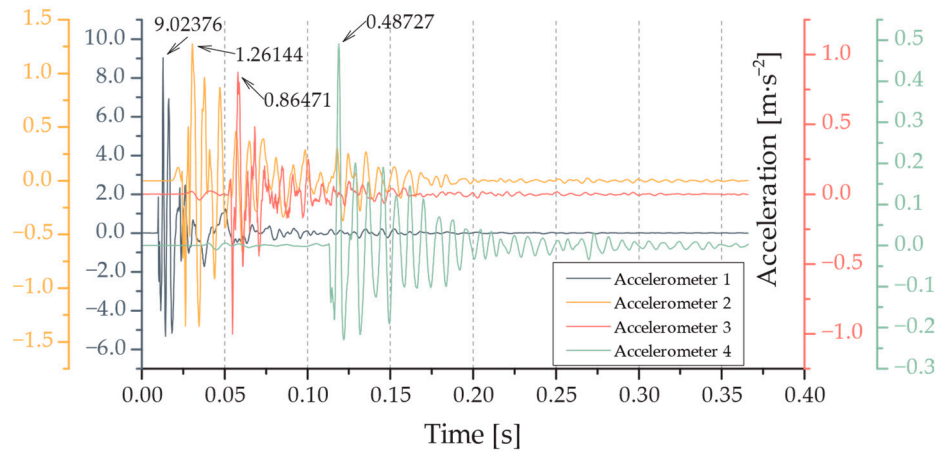


Figure 19. Measurement No. 7—military explosive V10b-el—vibration velocity time history of accelerometers 1 to 4 with indication of maximum acceleration values.

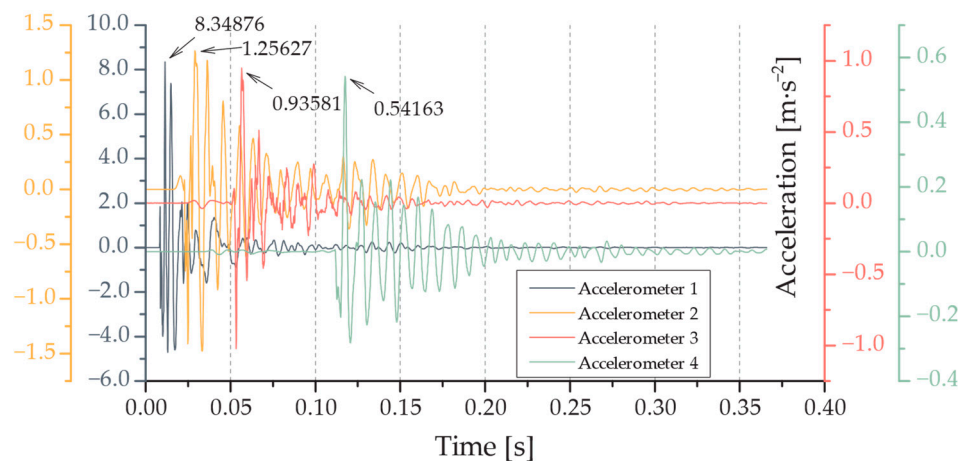


Figure 20. Measurement No. 8—military explosive V10b-el—vibration velocity time history of accelerometers 1 to 4 with indication of maximum acceleration values.

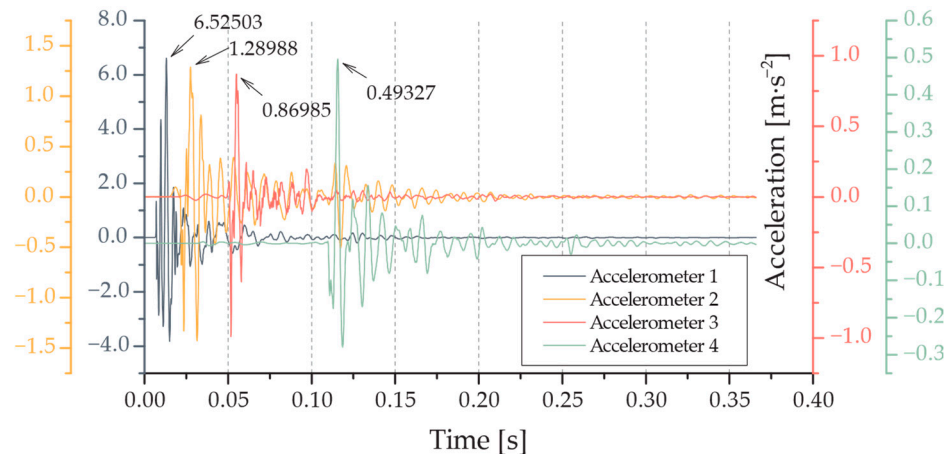


Figure 21. Measurement No.9—military explosive V10b-el (+ 1 m)—vibration velocity time history of accelerometers 1 to 4 with indication of maximum acceleration values.

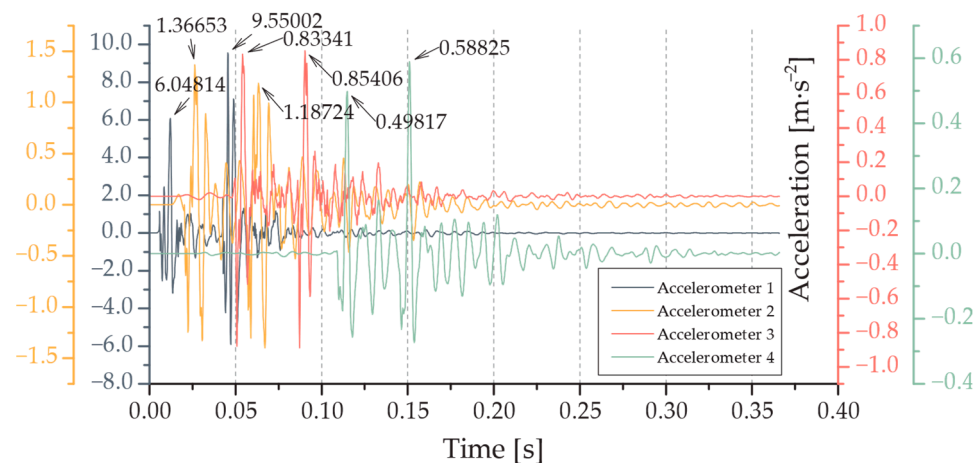


Figure 22. Measurement No.10—military explosive $2 \times$ V10b-el (+ 2 m)—vibration velocity time history of accelerometers 1 to 4 with indication of maximum acceleration values.

Figure 24 depicts the attenuation curves of the selected three measurements. The y-axis in the plot represents the maximum value of acceleration measured on a given accelerometer—the x-axis. In the plots, the trend line is the exponential function associated with the corresponding points. This function represents the trend of the data and predicts future values. However, it is important to note that the trend line does not have to intersect all points. This is often due to imperfections in the measuring equipment as well as large differences in the amplitudes of the measured values. Some values may be too small or too large to measure precisely. As a result, points may appear that are not in line with the trend line. In addition, the accuracy of the data may be affected by the physical capabilities of the measurement system.

The peak particle velocity (PPV) method is commonly used to assess the impact of vibration and potential damage to structures. It refers to the maximum velocity a particle reaches during a vibration-related event, usually measured in meters per second ($\text{m}\cdot\text{s}^{-1}$). In this case, the PPV analysis was performed on one measurement—measurement No. 9. However, as the measured values were in acceleration units ($\text{m}\cdot\text{s}^{-2}$), it was necessary to perform an analytical integration of the vibration acceleration time history (Figure 25) from all four accelerometers in order to compare the results with the available literature.

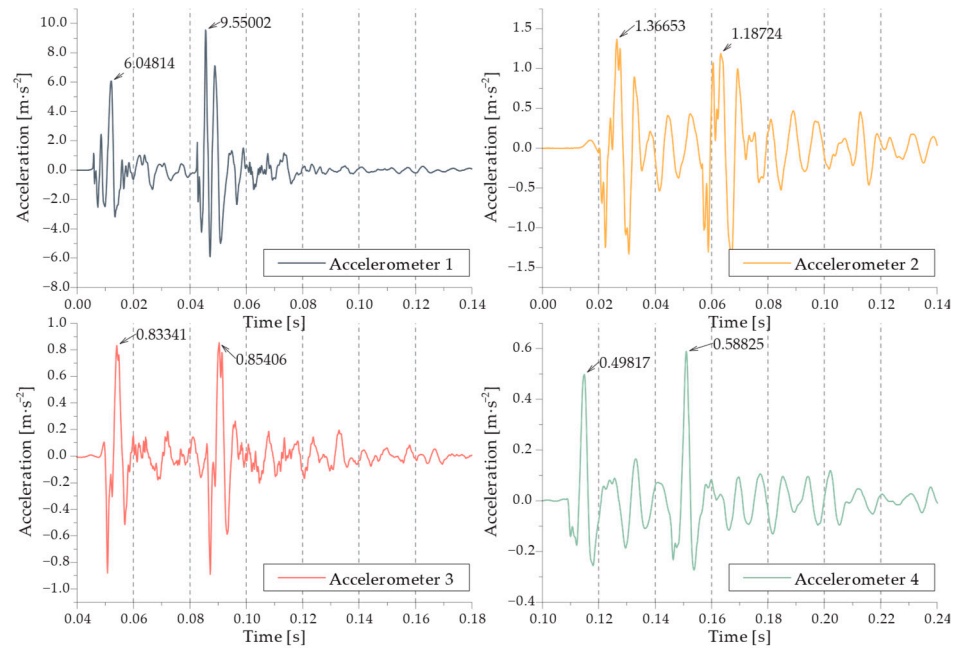


Figure 23. Measurement No. 10—military explosive 2 × V10b-el (+ 2 m)—vibration velocity time history of individual accelerometers 1 to 4 with indication of maximum acceleration values.

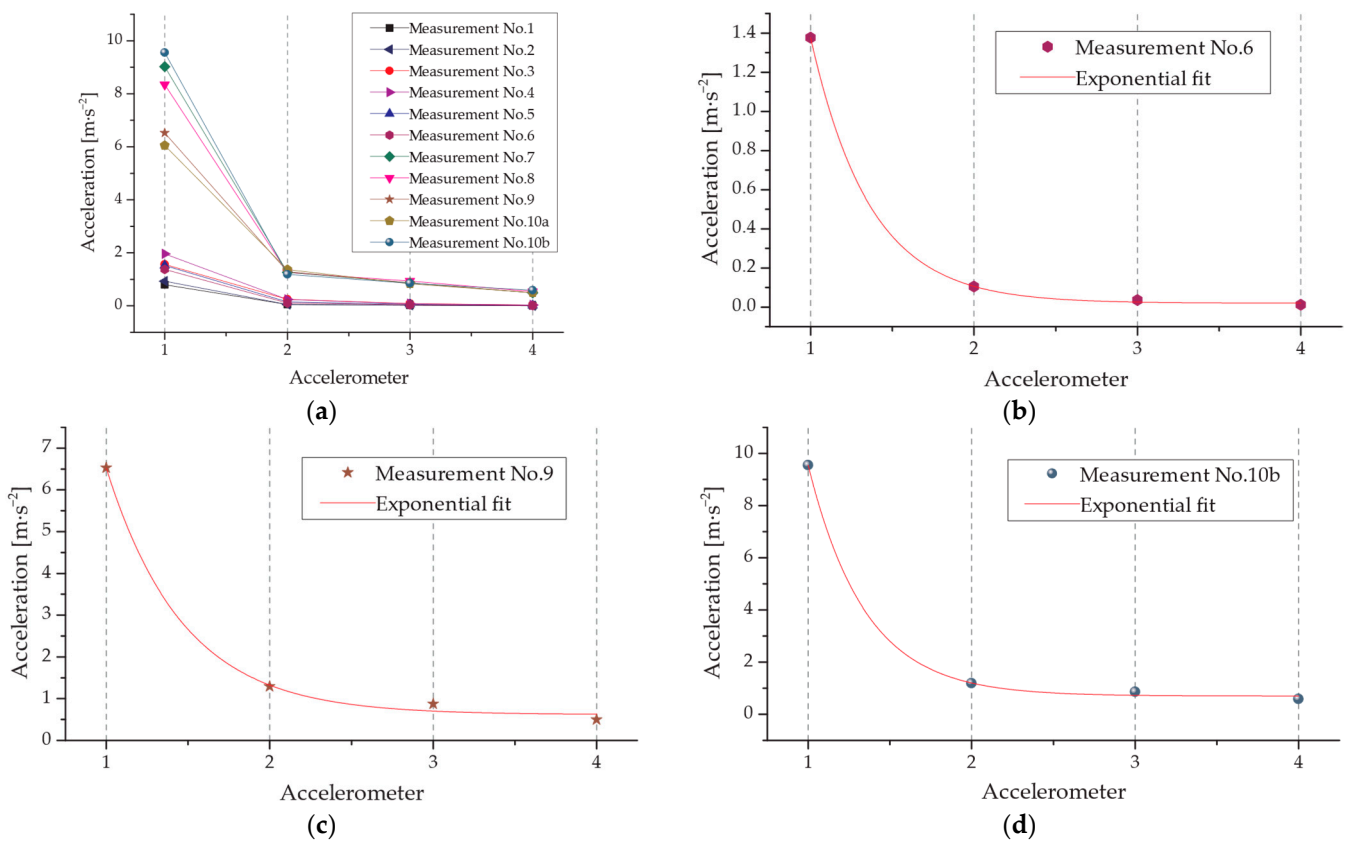


Figure 24. Attenuation curves from experimental measurements. (a) All measurements; (b) Viper 1 firecracker; (c) V10b-el military explosive; (d) 2 × V10b-el military explosive—maximum peaks No. 2.

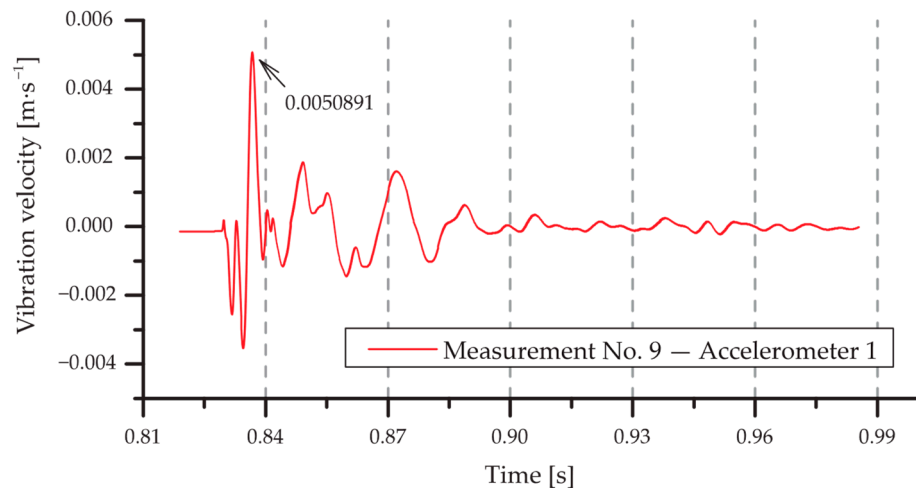


Figure 25. Analytical integration of the acceleration vibration waveform of accelerometer 1 from measurement No. 9 with maximum amplitude indicated.

After data integration, the highest amplitude values were identified and these were fitted with an exponential curve, as shown in Figure 26. The dispersive attenuation was confirmed and is consistent with existing research on this subject [13].

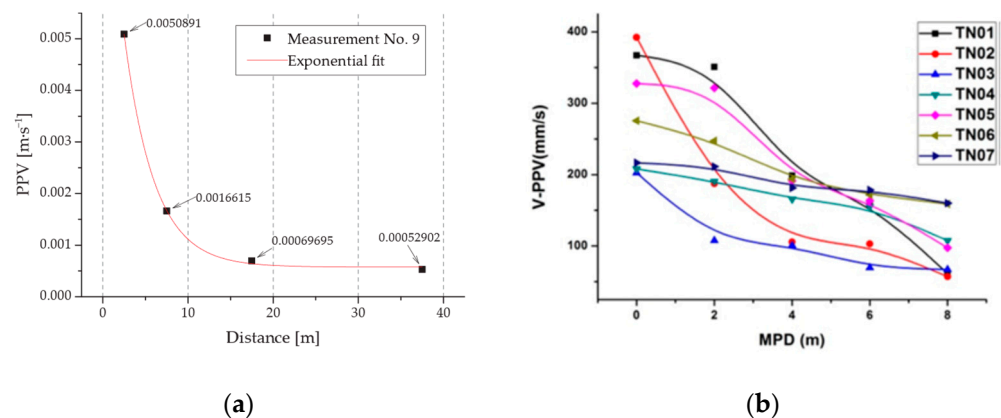


Figure 26. The comparison of our PPV results (a) with those published in the literature (b). (a) Peak particle velocity—measurement No. 9; (b) Attenuation relationship of vertical peak particle velocity [10].

The decrease in vibration amplitude with increasing distance can be attributed to two components: geometric attenuation and material attenuation, which can be described by the following equation:

$$y_n = y_1 \cdot \sqrt{\frac{x_1}{x_n}} \cdot e^{-\alpha(x_n - x_1)} \quad (1)$$

where, y_1 and y_n are the peak particle velocity at distances x_1 and x_n from the vibration source; e is the Euler's number, and α is the material attenuation coefficient [14].

After substituting the PPV and distance values, the material attenuation coefficient α can be calculated. For our measurements, the value of the material attenuation coefficient for the second and third accelerometers came out to be $\alpha_1 = 0.06389$, and for comparison, $\alpha_2 = -0.14487$ for the results from the available literature [13]. As the value of the attenuation coefficient increases, so does the overall attenuation. Accelerometer No. 2 has a lower PPV value than accelerometer No. 3 resulting in a negative attenuation coefficient value for the available literature, but this does not necessarily mean that the two measurements are not in agreement. In fact, a comparison of the two coefficients alone may not be sufficient to conclude whether the measurements are in agreement or not. A more comprehensive

analysis, including a larger set of measurements and a deeper examination of the data, would be needed to accurately assess the agreement between a pair of measurements.

Dynamic Scaling

Scaling is an important process that is applied in many sectors, including the construction industry. It involves the creation of a small-scale model that replicates the geometric properties and behavior of a large-scale model. Dynamic tests on the scaled model can provide important insights into the performance and response characteristics of the real model. The idea of scaling is based on the similarity principle, which states that when things are subjected to the same conditions, they will behave similarly if they are geometrically comparable. This technique enables the scaled model's characteristics to be utilized to forecast the model's behavior at full scale. The benefit is the ability to extrapolate the small-scale model's results and predict the model's future evolution and behavior in reality [15].

Previous research [16] has been carried out on a small-scale model to investigate the behavior of seismic waves generated by an explosion. The model consisted of two main parts: a section designed to place the simulation mass, and a vertical wall designed to prevent the reflection of acoustic waves (Figure 27). For practical reasons, polystyrene was chosen as the material. The simulation mass consisted of kinetic sand, which is a combination of 98% sand and 2% polydimethylsiloxane, a silicon-based organic polymer known for its viscous properties. It is viscoelastic, which means that over long periods of time (or at high temperatures) it behaves like a viscous liquid, similar to honey. However, over short time flows (or at low temperatures) it behaves as an elastic solid, like rubber [17].

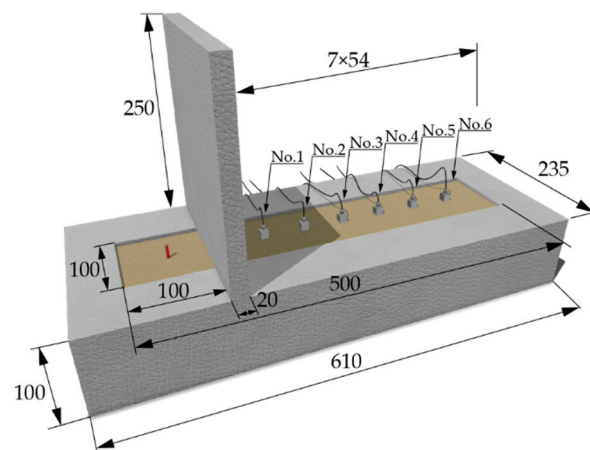


Figure 27. Three-dimensional visualization of the small-scale model that was used for the previous experimental measurements.

Six accelerometers were used for the measurements, which were evenly placed in the simulation mass, as shown in Figure 28. The axial distance between them was 54 mm. The firecrackers used were K01M Blasting Carpet with 0.05 g pyrotechnic composition per firecracker.

Figure 29 shows the vibration velocity time history for a small-scale experiment. The plot contains four separate graphs, each representing the acceleration data recorded by an individual accelerometer. The x-axis represents the time measured in seconds. The y-axis represents acceleration values measured in meters per second squared ($\text{m}\cdot\text{s}^{-2}$).

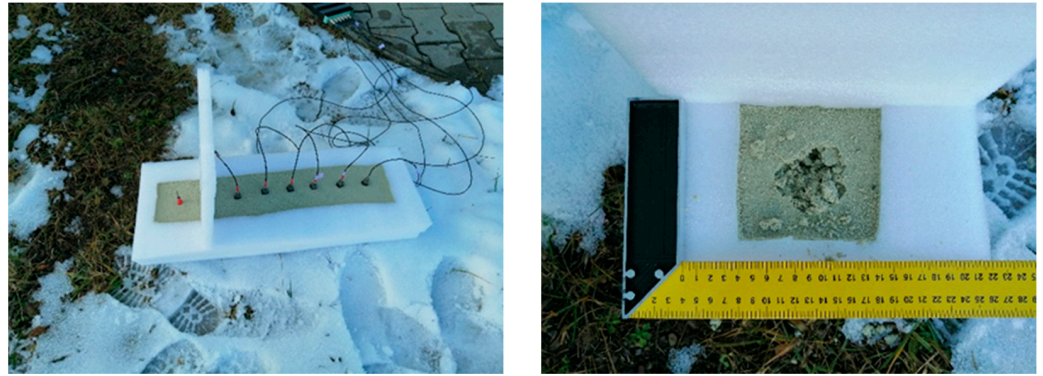


Figure 28. Small-scale model from a previous experimental measurement (left) and the result of a firecracker explosion (right).

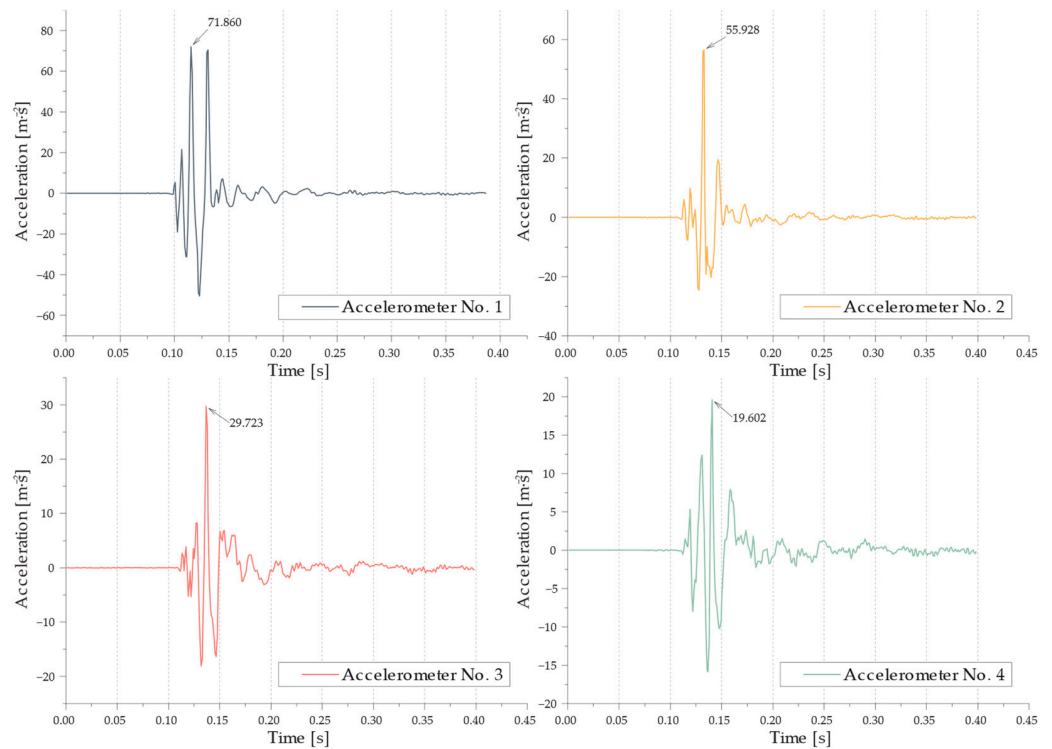


Figure 29. Vibration velocity time history of the first four accelerometers from experimental measurements on a small-scale model.

According to [18], the concept of dynamic exponent can be established to quantify the relationship between time and distance as follows:

$$\frac{t_2}{t_1} = \left(\frac{L_2}{L_1} \right)^z \quad (2)$$

where t is the time when the seismic wave arrived at the accelerometer, L is the distance of the accelerometers from the explosion source, index 1 represents the small-scale model, index 2 represents the full-scale model, and z is the dynamic exponent, which in this case will be used to represent the dependence between time and distance at different scales.

The following tables, Tables 1–3, present all the measured data from the experimental measurements for the different types of seismic waves.

Table 1. Real measured values from experimental measurements for the P-wave.

Accelerometer	Small-Scale Experiment		Full-Scale Experiment	
	Distance [cm]	Time [s]	Distance [cm]	Time [s]
1	12.4	0.027832022	350.000	0.00854548
2	17.8	0.031590762	1153.704	0.03014956
3	23.2	0.035975218	1957.408	0.05537665
4	28.6	0.039875242	2761.112	0.07877247

Table 2. Real measured values from experimental measurements for the S-wave.

Accelerometer	Small-Scale Experiment		Full-Scale Experiment	
	Distance [cm]	Time [s]	Distance [cm]	Time [s]
1	12.4	0.029872185	350.000	0.00928645
2	17.8	0.034587543	1153.704	0.02772267
3	23.2	0.038212599	1957.408	0.04284052
4	28.6	0.040852125	2761.112	0.07202703

Table 3. Real measured values from experimental measurements for the surface Rayleigh wave.

Accelerometer	Small-Scale Experiment		Full-Scale Experiment	
	Distance [cm]	Time [s]	Distance [cm]	Time [s]
1	12.4	0.031494153	350.000	0.01135010
2	17.8	0.032958973	1153.704	0.03751275
3	23.2	0.033935535	1957.408	0.05989980
4	28.6	0.034912097	2761.112	0.08429225

After plugging all the measured values into Equation (2), it is possible to calculate the dynamic exponent for each type of seismic wave. The results are summarized in Table 4.

Table 4. Resultant dynamic exponent values for each type of seismic wave.

Dynamic Exponent	P-Wave	S-Wave	Rayleigh Wave
z_1	−0.353695358	−0.349995024	−0.305542249
z_2	−0.011193578	−0.053036383	0.031023915
z_3	0.097250485	0.025775274	0.128113134
z_4	0.148973875	0.124088593	0.192879648

Scaling was accomplished by subtracting the time data for all seismic wave types from the graphs using a small-scale model for the first four accelerometers. Due to the fact that only four accelerometers were used for the full-scale experimental measurements, the last two accelerometers from the small-scale model were excluded and not considered in this analysis. In the next step, graphs were plotted in which the horizontal axis indicated the distance from the explosion location to each accelerometer, and the vertical axis represented the time at which the seismic wave reached the accelerometer, as shown in Figures 30–32. Based on the measurements collected during the experiment, a standard deviation was calculated to quantify the variability within the data set. This statistical value provides insight into how much the individual measurements differ from the average. The coefficient of determination was used to identify a functional relationship that accurately represents the interrelationship between time and distance. To express this relationship mathematically, a power function was determined to be the most appropriate for each type of seismic wave, as shown in Equations (3)–(5).

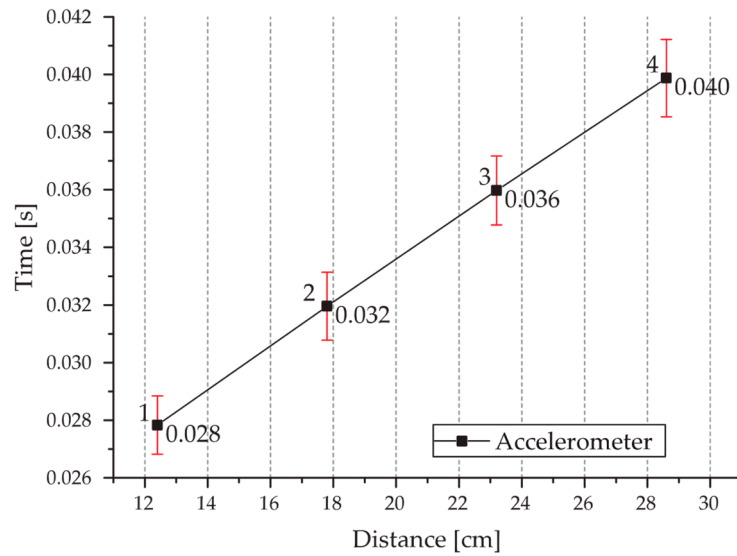


Figure 30. Graphical representation of the dependence of distance and time at each accelerometer for the P-wave propagation.

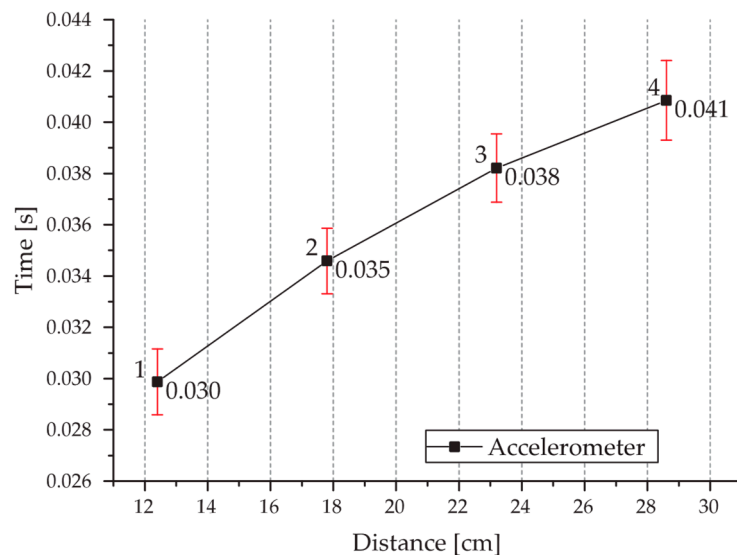


Figure 31. Graphical representation of the dependence of distance and time at each accelerometer for the S-wave propagation.

Power function for the P-wave propagation:

$$y = 0.0093 \cdot x^{0.4316} \quad (3)$$

Power function for the S-wave propagation:

$$y = 0.0116 \cdot x^{0.3769} \quad (4)$$

Power function for the surface Rayleigh wave propagation:

$$y = 0.0232 \cdot x^{0.1219} \quad (5)$$

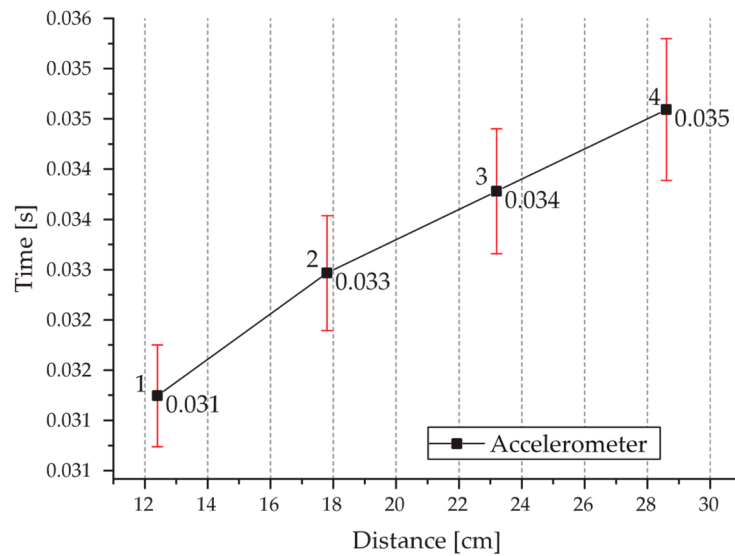


Figure 32. Graphical representation of the dependence of distance and time at each accelerometer for the surface Rayleigh wave propagation.

After obtaining the behavior and assuming further evolution on the small-scale model, by substituting the distance x from the full-scale model into the found function, the time when the seismic waves arrive at the accelerometer was calculated and then compared with the real measured data, as shown in Table 5. However, an initial adjustment was necessary for the distances within the full-scale model, and this was because the increase in distance between accelerometers does not follow a constant pattern as in the small-scale model. This adjustment was made by linear interpolation, which is a simple numerical method for determining the value of a measurand that is not within the interval of measured values.

Table 5. Theoretical values of times calculated by plugging distances into power functions for each seismic wave type.

Accelerometer	Distance [cm]	Time P-Wave [s]	Time S-Wave [s]	Time Rayleigh Wave [s]
1	350.000	0.11654743	0.10551573	0.04738161
2	1153.704	0.19502167	0.16540981	0.05479706
3	1957.408	0.24500368	0.20187970	0.05844454
4	2761.112	0.28422011	0.22982779	0.06094753

4. Discussion

The paper deals with the problem of wave propagation from explosions in geological environments. Brief mention has been made of how explosions occur and how the energy released propagates away from the source. The measurement technique and the pyrotechnics used, without which the experimental measurements could not have been carried out, are also described. The analysis of the signals on which the measurements were based is described in detail.

The model used in this study was designed to simulate the behavior of seismic waves generated by explosions in a controlled environment that closely resembles real geological conditions. The choice of model is critical for ensuring that the findings can be applied to real-world scenarios. The model incorporates various parameters that reflect the complexities of geological environments, including material properties and boundary conditions. By carefully selecting these parameters, the model accurately represents the dynamic response of geological materials to explosive forces.

Kinetic sand was specifically chosen for its unique properties, which closely resemble a real geological environment in the context of a small-scale model. The use of natural soil was not practical for these experiments due to the fact that grain sizes can vary, moisture levels are hard to control, and its density can differ widely. These variations make it challenging to achieve consistent and accurate results. Kinetic sand, on the other hand, offers a controlled and uniform medium that mimics the granular behavior of natural soil while allowing for more precise control over variables, ensuring that the experiments are both accurate and repeatable. Its viscoelastic properties enable it to absorb and dissipate energy, accurately simulating how geological materials respond to dynamic loads like explosions. Additionally, kinetic sand is easy to shape and manipulate, allowing researchers to create diverse experimental setups and explore various real-world conditions. The application of the model extends beyond mere simulation; it serves as a tool for predicting the effects of explosions on structures and the surrounding environment. The rationality of using kinetic sand lies in its ability to provide insights into the behavior of seismic waves in a medium that closely resembles natural conditions.

Our results show that the calculated attenuation coefficient deviates from previously performed studies due to differences in PPV values at each accelerometer. The graph (Figure 26) shows that the values of the third accelerometer towards the second accelerometer are increasing, which in our case is just the opposite. These results highlight the need to carefully consider the unique characteristics of the geological environment when conducting future investigations.

In the chapter on dynamic scaling, the calculation of the dynamic exponent, denoted as z , which in this case served as the scaling factor, was investigated. Two separate experiments were conducted, one using a small-scale model and the other using a full-scale model, and their results were compared.

However, there were several reasons why the theoretically calculated values did not match the actual measured values. The accelerometers themselves did not have a suitable scale and this factor significantly affected the results. On the small-scale model, the accelerometers appeared relatively large in terms of their mass, which led to deviations in the measured data. In addition, the stabilization of the accelerometers played a key role. On the small-scale model, steel bolts were used to stabilize the accelerometers, whereas on the larger-scale model, wooden stakes were used to stabilize the accelerometers. This difference in stabilization methods also caused a discrepancy in the results. The environment in which the experiments were conducted also had an influence. Despite efforts to simulate the same conditions as much as possible in the case of the small-scale model, it was not possible to achieve absolute agreement. In addition, the setup of the whole system also had an impact on the results. On the full-scale model, the cables closest to the blast source were additionally covered with sand to prevent any acoustic wave interference. Awareness of all these factors is crucial for accurate interpretation and understanding of experimental results. The presented problem has also been addressed by experts in Ljubljana, Slovenia; their results are found in [19–25]. It is possible to conduct an analysis of the scale effect using a mechanics-based equation in combination with classical attenuation laws, as presented in [26]. However, this approach will be addressed in future research.

5. Conclusions

In summary, the work provides insights into the behavior of seismic waves generated by explosions. It has been shown that all types of seismic waves (P-waves, S-waves, and surface waves) reached the accelerometers and propagated through the geological environment. At the same time, dispersive attenuation, a phenomenon in which high-frequency waves propagate faster than low-frequency waves, can also be observed, leading to a reduction in signal amplitude over larger distances. Our measurements show agreement with the results of previous foreign research, indicating a high degree of reliability of the methods and procedures used. The attenuation coefficient, which is an important parameter in characterizing the behavior of waves in a given environment, was also calculated.

The findings presented in this work are of fundamental importance for understanding the effects of explosions on nearby structures and the surrounding environment. With a detailed understanding of the behavior of seismic waves induced by explosions, we will be able to design building structures that can better withstand extraordinary dynamic loads. In general, this work provides an introduction to the issues in blast seismicity and provides a foundation for further research in this area. This practical research is currently being continued and the correlation of in situ results, numerical calculations, analytical assumptions, and actual full-scale experiments is very interesting and will soon also be presented in a scientific publication.

Author Contributions: Conceptualization, D.P. and Z.P.; methodology, E.B. and D.P.; software, D.P. and E.B.; validation, Z.P., D.P., and E.B.; formal analysis, Z.P.; investigation, E.B.; resources, E.B. and Z.P.; data curation, Z.P.; writing—original draft preparation, E.B.; writing—review and editing, Z.P. and D.P.; visualization, E.B.; supervision, Z.P.; project administration, D.P.; funding acquisition, D.P. All authors have read and agreed to the published version of the manuscript.

Funding: This research was funded by the Ministry of Education, Science, Research and Sport of the Slovak Republic, grant number VEGA 1/0552/24 “Adverse dynamic effects of transport on historic buildings and the possibilities of mitigating them with innovative materials in transport engineering”.

Data Availability Statement: The data presented in this study are available on request from the corresponding author. At the time the project was carried out, there was no obligation to make the data publicly available.

Acknowledgments: This research has been supported by the Project “SPS G5924—Inspection and security by Robots interacting with Infrastructure digital twinS (IRIS)”, approved in the framework of the NATO Science for Peace and Security (SPS) Programme.

Conflicts of Interest: The authors declare no conflicts of interest. The funders had no role in the design of the study; in the collection, analyses, or interpretation of data; in the writing of the manuscript; or in the decision to publish the results.

References

1. Wu, C.; Hao, H.; Lu, Y.; Zhou, Y. Characteristics of stress waves recorded in small-scale field blast tests on a layered rock–soil site. *Geotechnique* **2003**, *53*, 587–599. [CrossRef]
2. Busch, C.L.; Tarefder, R.A. Evaluation of appropriate material models in LS-DYNA for MM-ALE finite element simulations of small-scale explosive airblast tests on clay soils. *Indian Geotech. J.* **2017**, *47*, 173–186. [CrossRef]
3. Luccioni, B.M.; Ambrosini, D. Numerical assessment of blast effects scaling procedures. *Mec. Comput.* **2010**, *29*, 1161–1179.
4. Global Terrorism Database. Available online: <https://www.start.umd.edu/gtd/downloads/Codebook.pdf> (accessed on 9 July 2023).
5. Our World in Data. Available online: <https://ourworldindata.org/terrorism> (accessed on 9 July 2023).
6. Sokol, M.; Tvrda, K. *Dynamika Stavebných Konštrukcií*; Nakladateľstvo STU: Bratislava, Slovakia, 2011.
7. Fay, S. The Characterisation of Blast Loading for Shallow Buried Explosives. Doctoral Dissertation, University of Sheffield, Sheffield, UK, 2020.
8. ScienceNewsExplores. Available online: <https://www.sciencenewsforstudents.org/article/explainer-seismic-waves-come-different-flavors> (accessed on 9 July 2023).
9. Brüel & Kjær. Available online: <https://www.bksv.com/-/media/literature/Product-Data/bp2083.ashx> (accessed on 9 July 2023).
10. Brüel & Kjær. Available online: <https://www.bksv.com/-/media/literature/Product-Data/bp2215.ashx> (accessed on 9 July 2023).
11. Český Úřad pro Zkoušení Zbraní a Střeliva. Available online: <https://www.cuzzs.cz/cs/> (accessed on 9 July 2023).
12. Scribbr. Available online: <https://www.scribbr.com/statistics/pearson-correlation-coefficient/> (accessed on 9 July 2023).
13. Zhao, H.B.; Long, Y.; Li, X.H.; Lu, L. Experimental and numerical investigation of the effect of blast-induced vibration from adjacent tunnel on existing tunnel. *KSCE J. Civ. Eng.* **2016**, *20*, 431–439. [CrossRef]
14. Bornitz, G. *Über die Ausbreitung der von Großkolbenmaschinen Erzeugten Bodenschwingungen in Die Tiefe*; Springer: Berlin/Heidelberg, Germany, 2013.
15. Zhao, X. Fundamental Experimental Studies In Scaling, Blast Mitigation and Material Processing. Doctoral Dissertation, University of South Carolina, Columbia, SC, USA, 2013.

16. Papán, D.; Brozová, E.; Papánová, Z. Experimental Simulation of Deformation Effect Propagation Due to Explosion on the Surface of a Small-Scale Model. *Buildings* **2023**, *13*, 1566. [[CrossRef](#)]
17. Stem Mayhem. Available online: <https://www.stemmayhem.com/how-does-kinetic-sand-work/> (accessed on 9 July 2023).
18. Sapozhnikov, V.B.; Foufoula-Georgiou, E. Experimental evidence of dynamic scaling and indications of self-organized criticality in braided rivers. *Water Resour. Res.* **1997**, *33*, 1983–1991. [[CrossRef](#)]
19. Nujaim, M.; Belem, T.; Giraud, A. Experimental Tests on a Small-Scale Model of a Mine Stope to Study the Behavior of Waste Rock Barricades during Backfilling. *Minerals* **2020**, *10*, 941. [[CrossRef](#)]
20. Caçoilo, A.; Mourão, R.; Belkassam, B.; Teixeira-Dias, F.; Vantomme, J.; Lecompte, D. Blast wave assessment in a compound survival container: Small-scale testing. *Proceedings* **2018**, *2*, 540. [[CrossRef](#)]
21. Papán, D.; Valášková, V.; Drusa, M. Numerical and experimental case study of blasting works effect. In *IOP Conference Series: Earth and Environmental Science*; IOP Publishing: Bristol, UK, 2016; Volume 44, p. 052052.
22. Ainalis, D.; Kaufmann, O.; Tshibangu, J.P.; Verlinden, O.; Kouroussis, G. Modelling the source of blasting for the numerical simulation of blast-induced ground vibrations: A review. *Rock Mech. Rock Eng.* **2017**, *50*, 171–193. [[CrossRef](#)]
23. Trajkovski, J.; Kunc, R.; Perenda, J.; Prebil, I. Minimum mesh design criteria for blast wave development and structural response-MMALE method. *Lat. Am. J. Solids Struct.* **2014**, *11*, 1999–2017. [[CrossRef](#)]
24. Trajkovski, J.; Perenda, J.; Kunc, R. Blast response of Light Armoured Vehicles (LAVs) with flat and V-hull floor. *Thin-Walled Struct.* **2018**, *131*, 238–244. [[CrossRef](#)]
25. Trajkovski, J.; Kunc, R.; Prebil, I. Blast response of centrally and eccentrically loaded flat-, U-, and V-shaped armored plates: Comparative study. *Shock Waves* **2017**, *27*, 583–591. [[CrossRef](#)]
26. Sabetta, F.; Pugliese, A. Attenuation of peak horizontal acceleration and velocity from Italian strong-motion records. *Bull. Seismol. Soc. Am.* **1987**, *77*, 1491–1513.

Disclaimer/Publisher’s Note: The statements, opinions and data contained in all publications are solely those of the individual author(s) and contributor(s) and not of MDPI and/or the editor(s). MDPI and/or the editor(s) disclaim responsibility for any injury to people or property resulting from any ideas, methods, instructions or products referred to in the content.